Biosensors and Bioelectronics 216 (2022) 114651

Contents lists available at ScienceDirect

Biosensors and Bioelectronics

journal homepage: www.elsevier.com/locate/bios

Needle-integrated ultrathin bioimpedance microsensor array for early detection of extravasation

Rongzhou Lin [a,b,c], Yunxia Jin [a], Renee R. Li [d,e], Chengmei Jiang [b,f], Jianfeng Ping [f], Christopher J. Charles [d,e], Yong Lin Kong [g], John S. Ho [a,b,c,*]

[a] Institute for Health Innovation and Technology, National University of Singapore, Singapore, 117599, Singapore
[b] Department of Electrical and Computer Engineering, National University of Singapore, Singapore, 117583, Singapore
[c] The N.1 Institute for Health, National University of Singapore, Singapore, 117456, Singapore
[d] Cardiovascular Research Institute, National University Heart Centre, Singapore, 119074, Singapore
[e] Department of Surgery, Yong Loo Lin School of Medicine, National University of Singapore, Singapore, 119228, Singapore
[f] School of Biosystems Engineering and Food Science, Zhejiang University, Hangzhou, 310058, PR China
[g] Department of Mechanical Engineering, University of Utah, Salt Lake City, UT, 84112, USA

ARTICLE INFO

Keywords:
Extravasation
Bioimpedance
Needle-integrated
Microsensor array
Early detection

ABSTRACT

Extravasation is a common complication during intravenous therapy in which infused fluids leak into the surrounding tissues. Timely intervention can prevent severe adverse consequences, but early detection remains an unmet clinical need because existing sensors are not sensitive to leakage occurring in small volumes (< 200 μL) or at deep venipuncture sites. Here, an ultrathin bioimpedance microsensor array that can be integrated on intravenous needles for early and sensitive detection of extravasation is reported. The array comprises eight microelectrodes fabricated on an ultrathin and flexible polyimide substrate as well as functionalized using poly (3,4-ethylenedioxythiophene) and multi-walled carbon nanotubes. Needle integration places the array proximity to venipuncture site, and functional coating significantly reduces interface impedance, both enable the microsensors with high sensitivity to detect early extravasation. *In vitro* and *in vivo* experiments demonstrate the capability of the microsensors to differentiate various intravenous solutions from different tissue layers as well as identify saline extravasation with detection limit as low as 20 μL.

1. Introduction

In modern medical practices, an estimated 80% of patients receive intravenous therapy during their admission, such as administration of medications for chemotherapy, ionic fluids for rehydration, and nutrients for health rehabilitation (Waitt et al., 2004). However, intravenous therapy is generally associated with a common complication – extravasation – the leakage of infused fluids into the surrounding tissues (Schulmeister, 2007). Depending on the volume and content of the leakage, extravasation can lead to an inflammatory response that manifests in pain, swelling and erythema, which can progress to local or systemic infection, and in some rare cases pulmonary edema and amputation (Al-Benna et al., 2013; Reynolds et al., 2014). These adverse consequences can be prevented by timely detection and intervention as soon as extravasation occurs. At present, extravasation diagnosis in clinical settings primarily rely on well-trained clinicians to perform assessment of swelling and erythema around the infusion sites (Coyle et al., 2014; Kreidieh et al., 2016; Ong and Van Gerpen, 2020). However, these observations can be unreliable because they are subjective and depend on individual patient factors.

To provide objective detection of extravasation, a number of volumetric and surface approaches have been developed. Volumetric approaches rely on monitoring tissue optical (Lee and Lin, 2021; ivWatch, 2021) and bioimpedance properties (Bicen et al., 2018; Jeong et al., 2019). However, penetration of light (Wilson and Patterson, 2008; Bansal et al., 2018) and electrical field (Park et al., 2018; Bard et al., 2022) into tissues is limited by scattering and adsorption. These volumetric approaches require well alignment of the sensor to be close proximity to venipuncture sites to achieve low limit of detection (0.2 mL) (ivWatch, 2021), or large sensor dimension to provide sufficient depth and coverage at the compromising of the detection limit (> 2 mL) (Bicen et al., 2018). Surface approaches are capable of sensitively

* Corresponding author. Institute for Health Innovation and Technology, National University of Singapore, Singapore, 117599, Singapore.
E-mail address: johnho@nus.edu.sg (J.S. Ho).

https://doi.org/10.1016/j.bios.2022.114651
Received 10 June 2022; Received in revised form 4 August 2022; Accepted 18 August 2022
Available online 31 August 2022

measuring skin temperature (Matsui et al., 2017), pressure (Lee and Lin, 2021) and strain (Bicen et al., 2018; Lim et al., 2021), but having limited sensitivity to corresponding changes in subcutaneous tissues, which may result in delayed diagnosis. As a result, existing methods are unable to provide diagnosis until significant amounts of fluid have been extravasated, and especially do not address the need to detect extravasation when administering through deep central venous routes.

In contrast, needle-integration enables sensing elements close access to pathological sites. Recent advances in microfabrication and materials science have enabled the development of microsystems small enough to be mounted on medical needles for in situ and real-time evaluation of tissue mechanical (Yu et al., 2018) and optical (Lee et al., 2020) properties as well as for multiparameter sensing of biomolecules, temperature and pressure (Park et al., 2020a, 2020b, 2021). However, needle-integrated bioimpedance sensors rely on large electrodes with millimeter dimensions to minimize electrode polarization effect, at the cost of lowing spatial resolution and sensitivity (Park et al., 2018, 2020a, 2020b; Kim et al., 2017; Yun et al., 2018). Instead, coating electrodes with functional nanomaterials can significantly improve active surface area and electrochemical activity, which enable low interface impedance despite the small dimensions (Jahnke et al., 2013; Chen et al., 2017; Liu et al., 2020). But this method has not been demonstrated yet for bioimpedance sensing.

Here, we demonstrate a needle-integrated bioimpedance microsensor array to provide early detection of extravasation. The array consists of eight microelectrodes (diameter 50 μm) fabricated on an ultrathin and flexible polyimide substrate as well as functionalized with a mixture of poly(3,4-ethylenedioxythiophene) and multi-walled carbon nanotubes (PEDOT-MWCNT). The miniature design and compliant mechanics of the array facilitates the integration on a standard intravenous needle with negligible change to its diameter. Needle-integration enables the microsensors proximity to venipuncture sites and to detect leakage through surface wetting at the very early of extravasation. The PEDOT-MWCNT coating significantly reduces the electrode interface impedance, therefore enabling microsensors to well differentiate saline solutions with impedance covering human tissues as well as typical intravenous solutions from porcine tissues. *In vitro* and *in vivo* experiments demonstrate that saline extravasation as low as 20 μL can be detected with the principal component analysis of the sensors' bioimpedance spectra.

2. Materials and methods

2.1. Fabrication of needle-integrated ultrathin bioimpedance microsensors

Microsensors were fabricated by photolithography in clean room. Silicon wafers with an aluminum layer (500 μm / 1 μm) were used as process substrates and the aluminum served as a sacrificial layer to release the microsensors. The bottom and top encapsulation layers (10 μm thickness) were fabricated by patterning photosensitive polyimide (Durimide 7505, Fujifilm) in the following procedures: spin coated at 2000 rpm for 30 s, prebaked at 100 °C for 3 min, exposed to UV light (400 nm wavelength) with 300 mJ/cm^2 dose, post baked at 90 °C for 5 min, developed sequentially in HTRD2 and RER600 (Fujifilm) for 2 min each, and ended by curing in 350 °C N_2 atmosphere for 1 h. The Au/Ti layer was patterned by using positive photoresist (AZ1512, MicroChemicals) in the following procedures: spin coated at 1000 rpm for 70 s, prebaked at 100 °C for 2 min, exposed to UV light (365 nm wavelength) with 210 mJ/cm^2 dose, post baked at 115 °C for 50 s, developed in a MK400 aqueous solution for 5 min, deposited 20 nm Ti and 200 nm Au layer by magnetic sputtering, and lift-off the remained photoresist and corresponding metal layer by ultrasonic treatment in acetone for 10 min. The microsensors were released from the silicon wafer by anodically oxidizing the Al layer in 1 M NaCl solution, and then connected to flexible flat cables by pressure sensitive adhesives (9703, 3M).

Electrochemical deposition of PEDOT-MWCNT followed the materials and procedures reported in (Chen et al., 2020). The deposition was performed on an electrochemical workstation (SP-200, Bio-Logic Science Instruments) by using a conventional three-electrode system including a Ag/AgCl reference electrode and a Pt counter electrode. The PEDOT-MWCNT film was electropolymerized from a aqueous solution containing 9 mM EDOT (Sigma-Aldrich) and 0.25 mg/mL MWCNT (8 nm diameter, 0.5–2 μm length, Cheaptube Inc.) by using the chronopotentiometry technique (0.4 mA/cm^2 current density, 2000 s duration). The microsensor was integrated on medical-approval needles (Gauge 18, BD) by using epoxy adhesives (MED-301, EPO-TEK). To avoid the risk of covering the PEDOT-MWCNT layer by the epoxy adhesives, the pristine Au electrode is firstly adhered to the intravenous needle from the backside by a very thin layer of epoxy, followed by the electrochemical deposition process to coat the porous structure.

2.2. Morphological and electrochemical characterization

The surface morphology of the PEDOT-MWCNT film was examined by using a field emission scanning electron microscope (FESEM, Verios460, FEI) operated at 2 kV. Electrochemical impedance spectroscopy was used to characterize the microsensors by the SP-200 electrochemical workstation with the three-electrode system. The spectrum was measured in 1 × PBS using a direct current potential (0 mV amplitude versus reference electrode) and an alternating current sinusoid potential (10 mV amplitude) with frequency ranging from 1 Hz to 1 MHz. Bench experiments of measuring impedance spectrum in intravenous solutions and porcine tissues were performed under the same setting while using a two-electrode system with the microsensor as working electrode and the Pt wire as counter electrode.

2.3. In vivo animal experiments

The mice experiment was performed in 8–12 weeks male wild-type C57BL/6 mice acquired from Jackson Laboratory. The mice were anesthetized via intraperitoneal injection of ketamine/xylazine mixture in saline (100 mg/kg and 10 mg/kg), followed by subcutaneous injection of analgesic buprenorphine (0.1 mg/kg), and level of anesthesia was regularly monitored by testing of toe pinch reflexes. After the mice reached an adequate depth of anesthesia, the gauge-18 needle integrated with a microsensor array and the Pt wire were inserted subcutaneously and formed a two-electrode system to continuously measure tissue impedance. Five aliquots of 100 μL 0.9% NaCl were intermittently injected down the needle.

The pig experiment was performed in a 45 kg female Landrace cross pig acquired from the Singapore National Large-Animal Research Facility. The pig was premedicated with intramuscular ketamine (10 mg/kg), midazolam (0.6 mg/kg) and atropine (0.04 mg/kg), induced with 4% isoflurane, intubated and maintained with 1–2% isoflurane throughout the experiments. The needle-integrated microsensor array was inserted into left carotid and subcutaneous space over the right external oblique to simulate conventional injection and extravasation, respectively. The Pt wire was inserted subcutaneously around 10-cm apart from the needle to form a two-electrode system. Multiple aliquots of 100 μL 0.9% NaCl were intermittently injected down the needle.

The animals were euthanized after the experiments. All animal experiments conformed to the Guide for the Care and Use of Laboratory Animals published by the US National Institutes of Health, and the study protocols (R19–0782, R21-0377) were approved by Institutional Animal Care and Use Committee, National University of Singapore.

3. Results and discussions

3.1. Design of needle-integrated ultrathin bioimpedance microsensor array

Needle-integrated microsensors were developed to detect

extravasation via monitoring bioimpedance. Impedance spectrum is measured by a electrochemical impedance spectroscopy which comprises a needle-integrated microsensor as the working electrode and a millimeter-sized Pt wire (not shown here) acts as the counter electrode (Fig. 1A). The resulting spectrum primarily reflects impedance of the space around the microsensor because the impedance at the counter electrodes is negligible considering its large surface area and high electrochemical activity (Bard et al., 2022). The microsensor array is mounted on the front end of an intravenous needle, and gains close proximity to the venipuncture site during intravenous administration. The microsensor is able to differentiate blood samples from tissues, therefore facilitating placement of the microsensor right outside of veins. When extravasation happens, the infusing solution leaks from the vein and results in either direct wetting of the microsensor or gradual diffusion into the surrounding tissue. In either case, the dielectric permittivity and the ionic conductivity of the space around the microsensor is changed, which is reflected in the shift of impedance spectrum.

Fig. 1B shows a schematic illustration of the microsensor array. The array is composed of eight Au electrodes (only four are shown) with 50 μm diameter exposed sites and 400 μm interdistance, top and bottom polyimide encapsulation layer (20 μm thickness, 600 μm width), and a PEDOT-MWCNT coating layer. A Ti layer is used to increase adhesion between Au layer and polyimide substrate. The small dimensions of the electrodes enable the electric field to be focused in a small volume to provide high spatial resolution (Béduer et al., 2014). The PEDOT-MWCNT layer coated on the Au electrode significantly increases active surface area and enables low interface impedance despite the small dimensions (Chen et al., 2020; Luo et al., 2011; Zhou et al., 2013). An array of eight electrodes connected to a multiplexing provides opportunities to measure a large area of tissue along the needle, and also enables various stages of extravasation to be monitoring by scanning the array elements. The array is integrated on a gauge-18 (1.25 mm diameter) intravenous needle using a biocompatible epoxy adhesive (Fig. 1C). Compared to the needle, the thickness of the array is almost negligible (< 5%). Materials used in the needle-integrated microsensors have been demonstrated to be biocompatible (Chen et al., 2020; Luo et al., 2011; Zhou et al., 2013; EPO-TEK, 2022).

3.2. Characterization of bioimpedance microsensors

The bioimpedance microsensors were functionalized with a PEDOT-MWCNT layer to significantly improve the sensitivity. Scanning electron microscopy image confirms that the PEDOT-MWCNT composite forms a porous layer on exposed electrode sites (Fig. 2A). Prior studies have shown that this composite provides outstanding conductivity and chemically stability because the negatively charged MWCNT can act as a dopant to balance positive charges in PEDOT and increase the bonding strength to prevent delamination from the Au surface (Chen et al., 2020; Luo et al., 2011; Zhou et al., 2013). Compared with bare Au microsensors, the PEDOT-MWCNT microsensors significantly reduce the interface impedance, which is measured in a high-concentration solution 1 × PBS (Fig. 2B). As shown in the spectra, the impedance magnitudes at frequencies <1 kHz are reduced around two order of magnitude. The frequency response of the PEDOT-MWCNT microsensors is capacitive-resistive in which $|Z|$ decreases with frequency f from 1 Hz to about 100 Hz, and then becomes almost constant. In contrast, the bare Au microsensors exhibit a capacitive response across the entire measured spectrum. This frequency response suggests that the coating layer significantly increases the interface capacitance and minimizes the electrode polarization effect. The PEDOT-MWCNT coating is also highly robust against cycling measurement. The spectra remain constant during the 150 cycles of testing, and $|Z|$ at 10 kHz shows

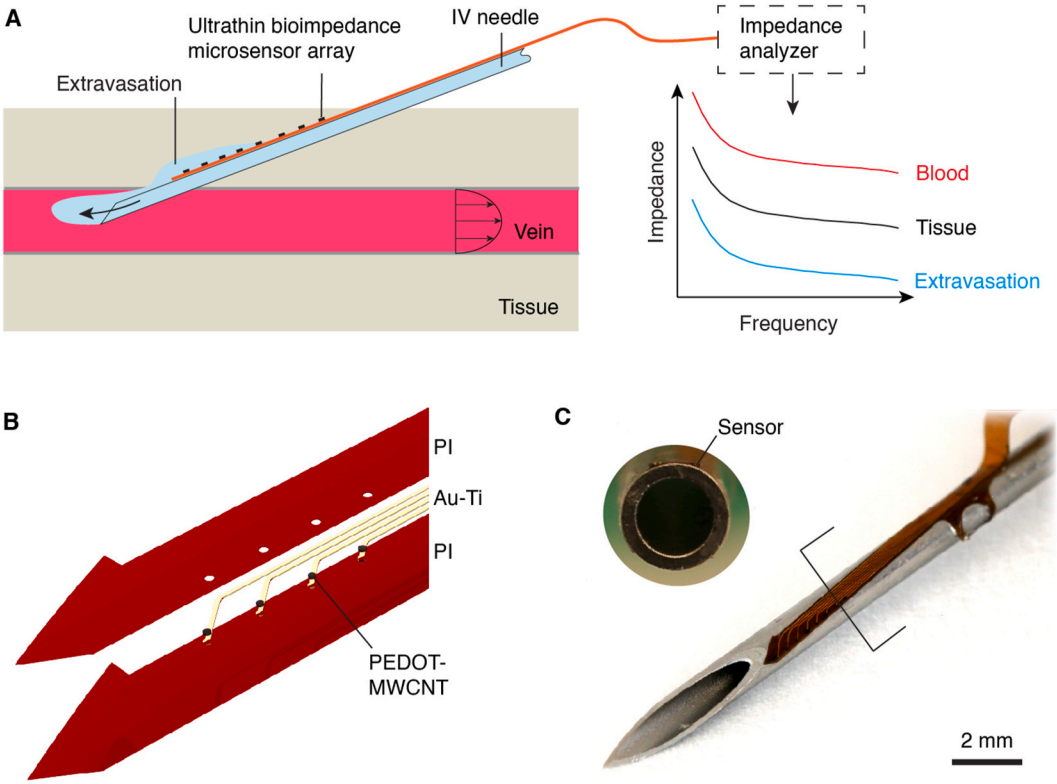

Fig. 1. Needle-integrated ultrathin microsensor array for detecting extravasation. A Illustration of the array mounted on an intravenous (IV) needle to gain proximity to the venipuncture site. Leakage of the infusing solution results in changes in the measured impedance spectrum due to wetting of the sensor surface. Impedance difference between blood and tissue facilitates the placement of microsensors outside of the vein. **B** Exploded-view of the microsensor array. The fabricated array has eight electrode sites; only four are shown here. PI, polyimide; PEDOT, poly(3,4-ethylenedioxythiophene); MWCNT, multi-walled carbon nanotube. **C** Photograph of the microsensor array mounted on a gauge-18 IV needle (1.25 mm diameter). Inset shows the cross-section of the needle.

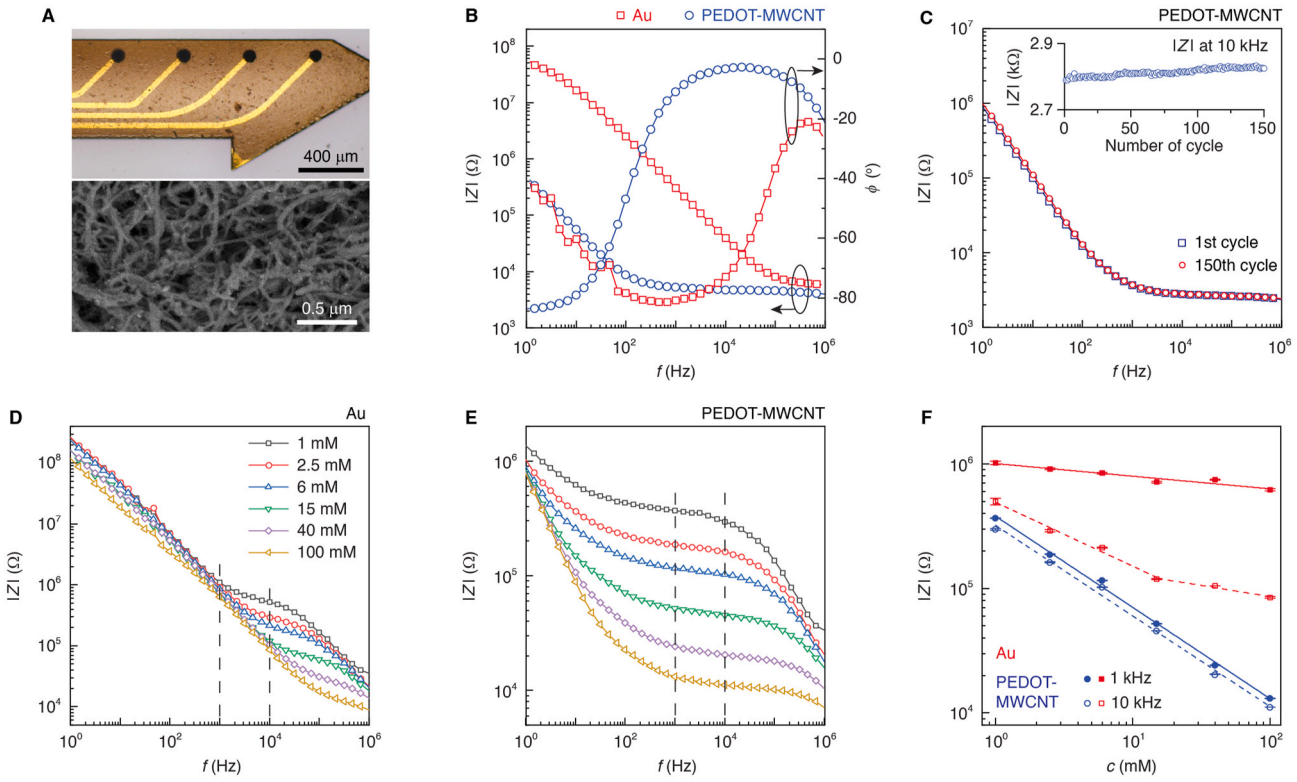

Fig. 2. Characterization of bioimpedance microsensors. A Optical and SEM images of PEDOT-MWCNT microsensors. SEM image shows microstructure of the coating. **B** Bode plots for Au and PEDOT-MWCNT microsensors. The plots are measured at 0 mV DC potential with 10 mV AC potential in 1 × PBS. $|Z|$, impedance magnitude. φ, phase angle. f, frequency. **C** Stability of the PEDOT-MWCNT microsensor against cycling measurement in 1 × PBS. Bode plots at the 1st and 150th cycle are shown for comparison. Inset shows dependence of $|Z|$ (at 10 kHz) on the number of measurement cycle. **D,E** Implementation of Au (**D**) and PEDOT-MWCNT (**E**) microsensors for measuring saline solution with concentration c ranging from 1 mM to 100 mM. **F** Dependence of $|Z|$ (at 1 kHz and 10 kHz) on c for Au and PEDOT-MWCNT microsensors. Error bar is mean ± s.d. ($n = 3$ measurements).

< 1.5% variation correspondingly (Fig. 2C).

Owing to the significant reduction in interface impedance, the PEDOT-MWCNT microsensors exhibit increased sensitivity to the properties of the surrounding environment. Fig. 2D–E show the impedance spectra measured by the bare Au and PEDOT-MWCNT microsensors in saline with concentration c varying from 1 to 100 mM, which covers the impedance range of most biological tissues (Park et al., 2018). The bare Au microsensors exhibit significantly overlapping spectra across the range of c, although some differentiation can be achieved around 10 kHz. In contrast, the impedance spectra acquired by the PEDOT-MWCNT microsensors are well-separated across frequencies ranging from 100 Hz to 100 kHz. To quantify the sensitivity, $|Z|$ at 1 kHz and 10 kHz are extracted and plotted versus c on a log-log scale (Fig. 2F). The PEDOT-MWCNT microsensor shows a linear slope -0.73 at both frequencies, while the Au microsensor shows a linear slope -0.1 at 1 kHz, but the slope changing from -0.513 to -0.177 at 10 kHz. It is challenge to employ Au microsensors on detecting low-impedance samples due to large electrode interface impedance. Across the concentration range, the relative impedance change $(|Z_{1mM}| - |Z_{100mM}|) / |Z_{100mM}|$ achieved by the PEDOT-MWCNT microsensor is about 41 and 5.3 times higher than that of the Au electrode at 1 kHz and 10 kHz, respectively. Overall, PEDOT-MWCNT microsensors achieve a much higher sensitivity across a wide range of impedance, and the sensitivity could be achieved at a single frequency, which suggests that the impedance analyzer can potentially be replaced by a low-cost and miniature device.

3.3. *In vitro porcine model evaluations*

We firstly evaluate impedance of intravenous solutions and porcine tissues in a two-electrode system (Fig. 3A). Specifically, we considered three widely used intravenous solutions: 0.9% Normal Saline (0.9% NaCl), Lactated Ringer's (LR) and 5% Dextrose in Water (D5W), which are used in intravenous therapy to restore or maintain normal fluid volume and electrolyte balance; as well as porcine tissues to model subcutaneous skin, fat, and muscle layers, which cover a range of cell types, densities, and extracellular fluid level. Measurement at each kind of sample is repeated for three technical trails, namely repeating the measurement procedure for three times. The samples are well-differentiated across multiple trials by the impedance magnitude $|Z|$ ranging from 1 kHz to 100 kHz (Fig. 3B) and also by phase angle φ from 10 Hz to 1 kHz (Fig. 3C). In this frequency range, the intravenous ionic solutions (0.9% NaCl and LR) exhibit the lowest impedance, followed by muscle, fat and skin, while the molecular solution (D5W) shows about two order of magnitudes higher impedance. The ionic solutions have similar ion concentration (308 mM and 246 mM) as extracellular fluids, therefore their impedance lies in the range of biological tissues. In contrast, dextrose exists in water as molecular that doesn't transfer current and therefore demonstrates much lower conductivity. Importantly, the microsensor can distinguish not only intravenous fluids from porcine tissues but also different type of tissues. This suggests the potential of the sensor for guiding needle during insertion in addition to providing extravasation detection.

We next evaluated the needle-integrated PEDOT-MWCNT microsensors on detecting extravasation *in vitro*. We simulated extravasation by intermittently dosing 0.9% NaCl into porcine muscle, which have close impedance and therefore making the detection to be challenge. Fig. 3D–E show the impedance spectrum and impedance at 10 kHz as a function of time during injecting the saline in steps of 20, 30, 50, 50 and 50 μL. The impedance measurements reveal a clear change in the spectrum when injecting as low as 20 μL saline. This detection limit is

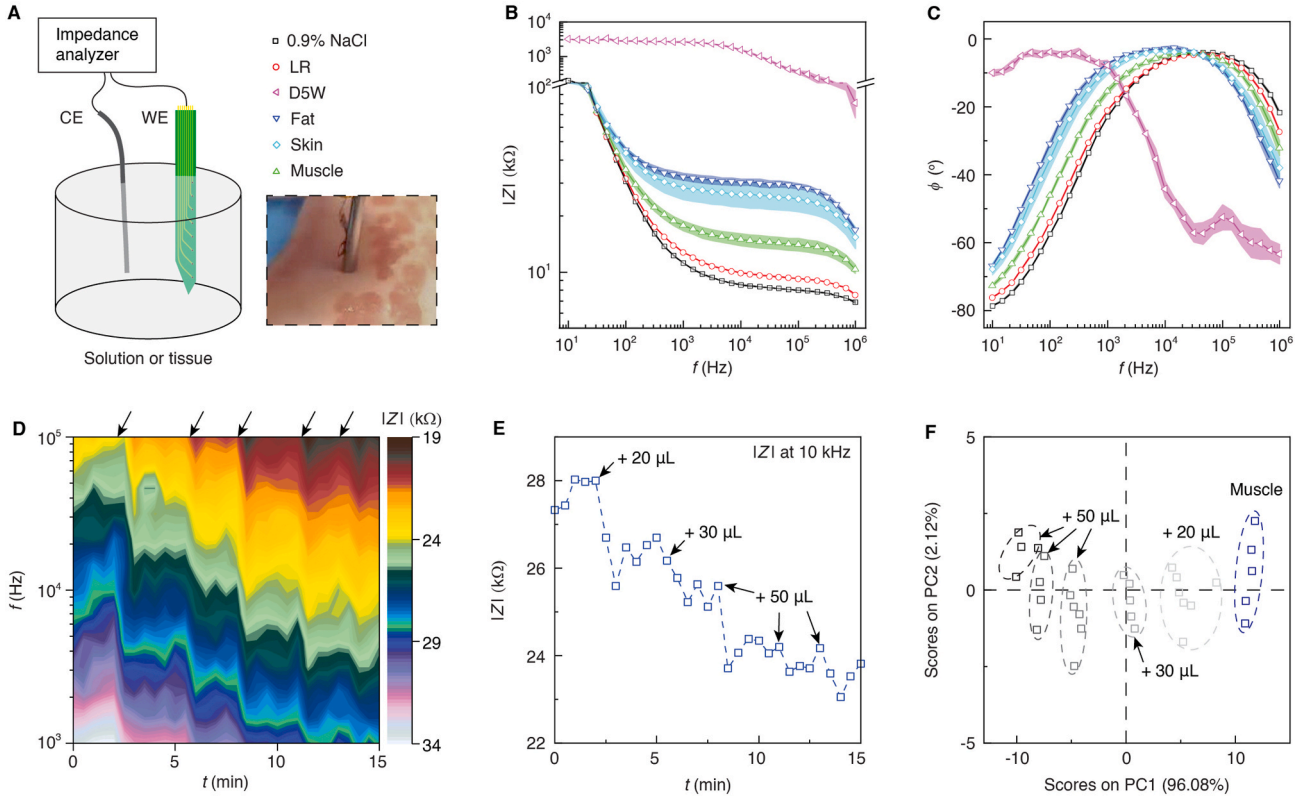

Fig. 3. ***In vitro*** **detection of extravasation in porcine tissues. A** Schematic illustration of a two-electrode system in which the microsensor and Pt wire is used as working electrode (WE) and counter electrode (CE), respectively. Tested subjects include typical intravenous solutions 0.9% Normal Saline (0.9% NaCl), Lactated Ringer's (LR) and 5% Dextrose in Water (D5W), as well as porcine fat, skin and muscle. Labels are applicable to (**B-C**). Inset picture shows the needle-integrated microsensor array is inserted into the porcine tissue. **B,C** Quantitative measurement results of the representative samples. Error bar is plotted as shadow, mean ± s.d. ($n = 3$ technical trials). **D,E** Impedance spectra (**D**) and impedance at 10 kHz $|Z|$ (**E**) as a function of time during intermittent injection of 0.9% NaCl in steps of 20, 30, 50, 50, 50 µL at time points indicated by the arrows. **F** Principal component analysis using the impedance spectra in (**D**).

about two order of magnitude lower than the best result achieved by current bioimpedance methods (Bicen et al., 2018). The change in $|Z|$ increases as more saline is infused, and saturates after about 100 µL injection. This saturation range is affected by the impedance difference between the tissue and dosing solution, the diffusion rate of ions, and sensor dimensions. We further used principal component analysis (PCA) to analyze the separability of the data sets collected by the microsensors. Fig. 3F shows that porcine muscles could be well separated from the cluster with saline injection using only the first principal component of the magnitude data. Alternatively, using an equivalent circuit model composed of a constant phase element (electrode interface) in series to a parallel resistor (fluids) and a capacitor (cells) to fit the impedance spectra (Kim et al., 2017; Zhou et al., 2013), the resistor element is found to provide the most differentiation between the samples. These *in vitro* experiments validate the ability of the microsensor to sensitively detect small volumes of extravasation, even when the infused solution has impedance in the range of biological tissues.

3.4. *In vivo animal model evaluations*

We demonstrated operation of microsensors *in vivo* using subcutaneous injection to model extravasation in mice and compared the sensor performance with visual assessment method. Mice were used in the visual assessment method as they have thin skin for easy observation of swelling. Fig. 4A shows images of the injection site (left thigh root) and the change in pixel intensity during five intermittent injections of 100 µL saline. However, the swelling from 100 µL injection is difficult to be detected even after subtracting the frame. Clinical extravasation of such volumes is not expected to be visually observable as the infusion site is located in regions much deeper under the skin and movement makes the image subtraction more challenge. In contrast, impedance spectra show significant responses to the injection, beginning from the first 100 µL injection and saturating after the third injection (Fig. 4B). Measurements at 10 kHz show that of $|Z|$ decreases from ~36.2 kΩ to ~33.8 kΩ with first 100 µL injection, and becomes saturated at approximately ~30.5 kΩ with 300 µL injection (Fig. 4C). Principal component analysis of the spectrum shows that $|Z|$ recorded under different injection volume form well-separated clusters, and that the separation between injection cluster and non-injection cluster increases with the infused volume (Fig. 4D).

We next demonstrated operation of microsensor array *in vivo* in a pig model. The needle-integrated microsensor array was inserted into left carotid and subcutaneous space over the right external oblique to monitor impedance variation of blood and tissue with injecting saline solution, respectively. (Fig. 5A). The impedance spectra were measured as a function of time during intermittent delivery of normal saline two times in steps of 100 µL. During conventional injection, the injected saline is rapidly taken away by the flow of blood in the vessel, therefore the spectra remain almost constant (Fig. 5B). In contrast, when saline is accumulated within the subcutaneous tissue, the spectra for tissues exhibit a clear change with the first injection of 100 µL saline (Fig. 5C). To be more specific, measurements at 10 kHz show that of $|Z|$ in blood vessel remains at ~50.0 kΩ while $|Z|$ at tissue reduces from ~36.1 kΩ to ~17.3 kΩ (Fig. 5D). The impedance variation caused by extravasation is also detected by three consecutive microsensors in the array (Fig. 5E). These results show that the needle-integrated microsensor can distinguish small volumes of extravasation from subcutaneous tissues *in vivo*. The capability to detect impedance difference between the blood and

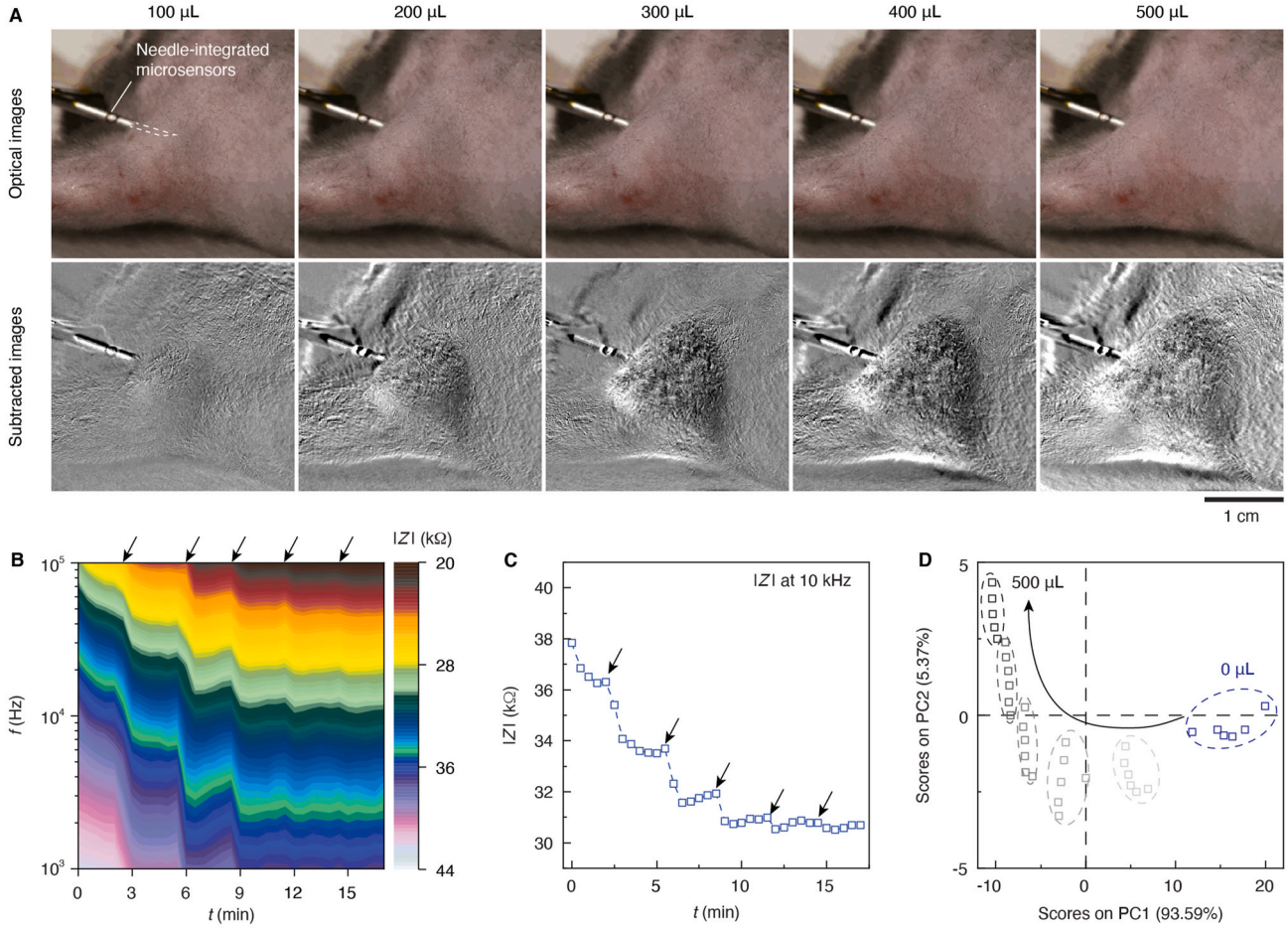

Fig. 4. ***In vivo*** **detection of extravasation in a mouse model. A** Optical images of the injection site (left thigh root in a mouse model) during infusion of 100 ~500 μL 0.9% NaCl. Subtracted images are shown to highlight swelling around the infusion site. White dash line indicates position of the needle-integrated microsensor under the skin. The needle diameter is 1.25 mm. **B,C** Impedance spectra (**B**) and impedance at 10 kHz |*Z*| (**C**) as a function of time during intermittent injection of 100 μL NaCl at time points indicated by the arrows. **D** Principal component analysis using the impedance spectra in (**B**).

tissue could facilitate the positioning of microsensors just outside of the blood vessel and near the venipuncture site.

4. Conclusions

We have demonstrated a needle-integrated ultrathin bioimpedance microsensor array capable of detecting early extravasation. The array was developed by using photolithography to pattern Au electrodes (50 μm diameter) on a flexible polyimide substrate (20 μm thickness, 600 μm width) and further by using electrochemical deposition to coat the Au electrodes with a porous PEDOT-MWCNT layer. The microelectrodes focus electric field in a small volume to provide high spatial resolution, and the PEDOT-MWCNT coating layer significantly increases active surface area and enables low interface impedance despite the small dimensions. The PEDOT-MWCNT microsensors capable of quantitatively differentiating saline solution with concentration ranging from 1 mM to 100 mM, which covers impedance of human tissues, as well as differentiating typical intravenous fluids (0.9% NaCl, LR and D5W) and porcine tissues (muscle, fat and skin). The miniature design and compliant mechanics facilitate integration of the microsensor array on standard intravenous needles (1.25 mm diameter) with negligible change (~ 5%) to the diameter of the needle. In contrast to existing non-invasive methods, needle-integration enables the microsensors proximity to the venipuncture sites and to detect extravasation at the very early stage. *In vitro* experiments show that the microsensor is able to detect local impedance change of porcine muscle with injecting as low as 20 μL 0.9% NaCl. Furthermore, *in vivo* experiments demonstrate that the microsensor can detect subcutaneous injection of solution before visual assessment of skin swelling in a mouse model and sensitively differentiate extravasation from conventional injection in a pig model. These results highlight the potential of using the needle-integrated ultrathin bioimpedance microsensors to monitor intravenous therapy, as well as integrating microsensors on other medical devices (Bai et al., 2018; Kalidasan et al., 2021) to address clinical challenges. Clinical use of these microsensors will require further validation of accuracy and safety, and the development of wireless and portable impedance analysis devices.

Credit authorship contribution statement

Rongzhou Lin: Conceptualization, Methodology, Formal analysis, Investigation, Data Curation, Writing - Original Draft, Visualization. **Yunxia Jin**: Methodology, Investigation. **Renee R. Li**: Methodology, Investigation. **Chengmei Jiang**: Methodology, Investigation. **Jianfeng Ping**: Supervision. **Christopher J. Charles**: Methodology, Resources, Supervision. **Yong Lin Kong**: Writing - Review & Editing, Supervision, Visualization. **John S. Ho**: Conceptualization, Methodology, Formal analysis, Resources, Writing - Review & Editing, Supervision, Funding acquisition, Visualization.

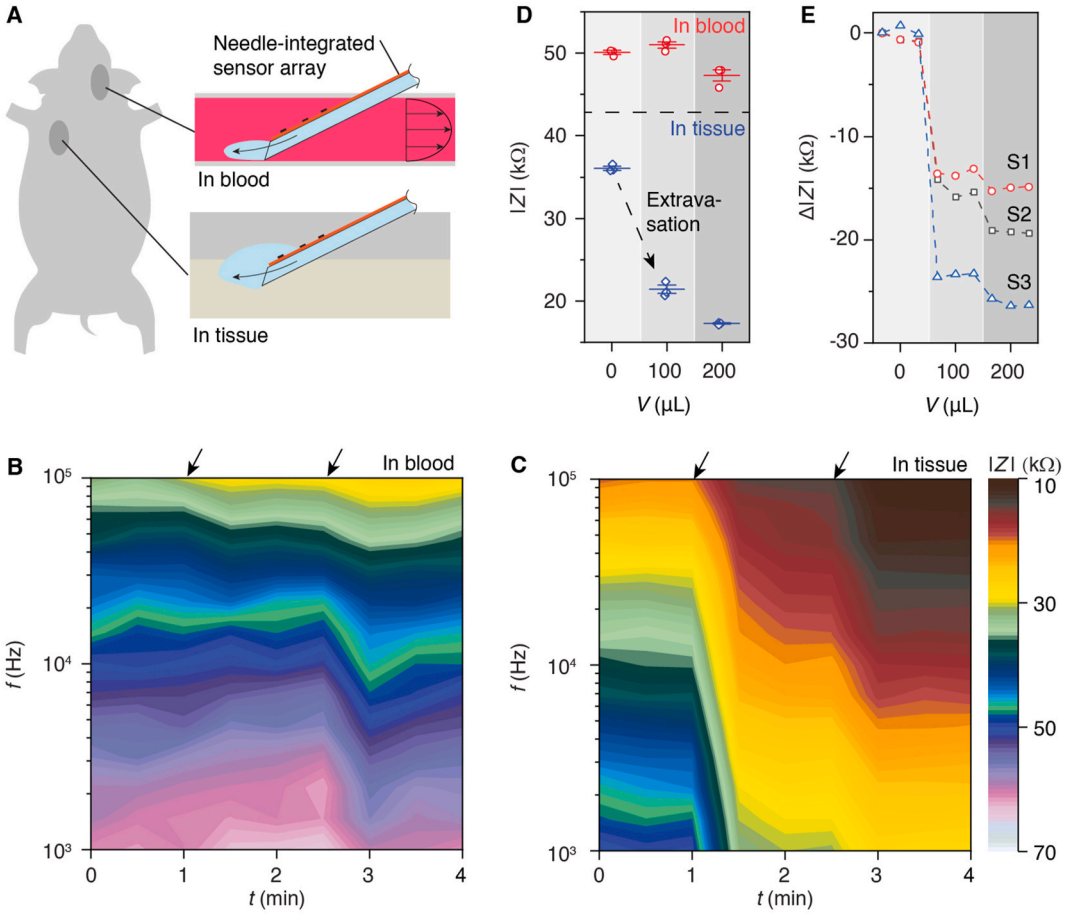

Fig. 5. ***In vivo*** **detection of extravasation in a pig model. A** Schematic illustration of impedance sensing in blood and in tissue during infusing 0.9% NaCl into left carotid and subcutaneous space over the right external oblique of a pig model, respectively. Tissue injection is used to simulate extravasation. **B,C** Impedance spectra obtained by the same microsensor in blood (**B**) and in tissue (**C**) as a function of time during intermittent injection of 100 μL saline at time points indicated by the arrows. Same color bar is used for (**B,C**). **D** Comparison of impedance $|Z|$ at 10 kHz against infusion of saline into blood and tissue. Error bar shows mean ± s.d. ($n = 3$ measurements). **E** The impedance change at 10 kHz $\triangle|Z|$ detected by three consecutive microsensors S1-S3 during extravasation.

Declaration of competing interest

The authors declare that they have no known competing financial interests or personal relationships that could have appeared to influence the work reported in this paper.

Data availability

Data will be made available on request.

Acknowledgments

J.S.H. acknowledges support from the National Research Foundation Singapore (Grant No. NRF-NRFF2017-07) and the Ministry of Education Singapore (Grants No. MOE2016-T3-1-004).

References

Al-Benna, S., O'Boyle, C., Holley, J., 2013. Extravasation injuries in adults. Int. Sch. Res. Notices 2013.
Bai, W., et al., 2018. Patchable micro/nanodevices interacting with skin. Biosens. Bioelectron. 122, 189–204.
Bansal, A., Yang, F., Tian, X., Zhang, Y., Ho, J.S., 2018. In vivo wireless photonic photodynamic therapy. Proc. Natl. Acad. Sci. USA 115, 1469–1474.
Bard, A.J., Faulkner, L.R., White, H.S., 2022. Electrochemical Methods: Fundamentals and Applications. John Wiley & Sons.
Béduer, A., et al., 2014. Accurate resistivity mouse brain mapping using microelectrode arrays. Biosens. Bioelectron. 60, 143–153.
Bicen, A.O., West, L.L., Cesar, L., Inan, O.T., 2018. Toward non-invasive and automatic intravenous infiltration detection: evaluation of bioimpedance and skin strain in a pig model. IEEE J. Translat. Eng. Health Med. 6, 1–7.
Chen, N., et al., 2017. Neural interfaces engineered via micro-and nanostructured coatings. Nano Today 14, 59–83.
Chen, N., et al., 2020. Nanotunnels within poly (3, 4-ethylenedioxythiophene)-carbon nanotube composite for highly sensitive neural interfacing. ACS Nano 14, 8059–8073.
Coyle, C.E., Griffie, J., Czaplewski, L.M., 2014. Eliminating extravasation events. J. Infusion Nurs. 37, 157–164.
EPO-TEK. MED-301 Technical data sheet. https://www.epotek.com/docs/en/Datasheet/MED-301.pdf. (Accessed 24 July 2022).
ivWatch, 2021. Early Detection of Iv Infiltration and Extravasation: Ivwatch Iv Monitoring. https://www.ivwatch.com/. (Accessed 6 June 2021).
Jahnke, H.-G., et al., 2013. Impedance spectroscopy—an outstanding method for label-free and real-time discrimination between brain and tumor tissue in vivo. Biosens. Bioelectron. 46, 8–14.
Jeong, I.S., et al., 2019. Detection of intravenous infiltration using impedance parameters in patients in a long-term care hospital. PLoS One 14, e0213585.
Kalidasan, V., et al., 2021. Wirelessly operated bioelectronic sutures for the monitoring of deep surgical wounds. Nat. Biomed. Eng. 1–11.
Kim, H.W., Yun, J., Lee, J.Z., Shin, D.G., Lee, J.-H., 2017. Evaluation of electrical impedance spectroscopy-on-a-needle as a novel tool to determine optimal surgical margin in partial nephrectomy. Adv. Healthcare Mater. 6, 1700356.
Kreidieh, F.Y., Moukadem, H.A., Saghir, N.S.E., 2016. Overview, prevention and management of chemotherapy extravasation. World J. Clin. Oncol. 7, 87.
Lee, H.-C., Lin, J.-S., 2021. An open-source wearable sensor system for detecting extravasation of intravenous infusion. IEEE Trans. Instrum. Meas. 70, 1–11.
Lee, S.Y., et al., 2020. Needle-compatible miniaturized optoelectronic sensor for pancreatic cancer detection. Sci. Adv. 6, eabc1746.
Lim, R., Damalerio, R.B., Bong, C.L., Tan, S.K., Cheng, M.-Y., 2021. Novel conformal skin patch with embedded thin-film electrodes for early detection of extravasation. Sensors 21, 3429.

Liu, S., Zhao, Y., Hao, W., Zhang, X.-D., Ming, D., 2020. Micro-and nanotechnology for neural electrode-tissue interfaces. Biosens. Bioelectron. 170, 112645.
Luo, X., Weaver, C.L., Zhou, D.D., Greenberg, R., Cui, X.T., 2011. Highly stable carbon nanotube doped poly (3, 4-ethylenedioxythiophene) for chronic neural stimulation. Biomaterials 32, 5551–5557.
Matsui, Y., et al., 2017. Evaluation of the predictive validity of thermography in identifying extravasation with intravenous chemotherapy infusions. J. Infusion Nurs. 40, 367.
Ong, J., Van Gerpen, R., 2020. Recommendations for management of noncytotoxic vesicant extravasations. J. Infusion Nurs. 43, 319–343.
Park, J., et al., 2018. Biopsy needle integrated with electrical impedance sensing microelectrode array towards real-time needle guidance and tissue discrimination. Sci. Rep. 8, 1–12.
Park, J., et al., 2020a. Biopsy needle integrated with multi-modal physical/chemical sensor array. Biosens. Bioelectron. 148, 111822.
Park, J., et al., 2020b. Microscale biosensor array based on flexible polymeric platform toward lab-on-a-needle: real-time multiparameter biomedical assays on curved needle surfaces. ACS Sens. 5, 1363–1373.
Park, J., et al., 2021. Real-time internal steam pop detection during radiofrequency ablation with a radiofrequency ablation needle integrated with a temperature and pressure sensor: preclinical and clinical pilot tests. Adv. Sci. 8, 2100725.
Reynolds, P.M., MacLaren, R., Mueller, S.W., Fish, D.N., Kiser, T.H., 2014. Management of extravasation injuries: a focused evaluation of noncytotoxic medications. Pharmacotherapy 34, 617–632.
Schulmeister, L., 2007. Infiltration and extravasation. Am. J. Nurs. 107, 16.
Waitt, C., Waitt, P., Pirmohamed, M., 2004. Intravenous therapy. Postgrad. Med. 80, 1–6.
Wilson, B.C., Patterson, M.S., 2008. The physics, biophysics and technology of photodynamic therapy. Phys. Med. Biol. 53, R61.
Yu, X., et al., 2018. Needle-shaped ultrathin piezoelectric microsystem for guided tissue targeting via mechanical sensing. Nat. Biomed. Eng. 2, 165–172.
Yun, J., Hong, Y.-T., Hong, K.-H., Lee, J.-H., 2018. Ex vivo identification of thyroid cancer tissue using electrical impedance spectroscopy on a needle. Sensor. Actuator. B Chem. 261, 537–544.
Zhou, H., Cheng, X., Rao, L., Li, T., Duan, Y.Y., 2013. Poly (3, 4-ethylenedioxythiophene)/multiwall carbon nanotube composite coatings for improving the stability of microelectrodes in neural prostheses applications. Acta Biomater. 9, 6439–6449.